Role of boric acid in synthesis and tailoring the properties of calcium aluminate phosphor

ARTICLE *in* MATERIALS CHEMISTRY AND PHYSICS · MARCH 2006

Impact Factor: 2.26 · DOI: 10.1016/j.matchemphys.2006.03.003

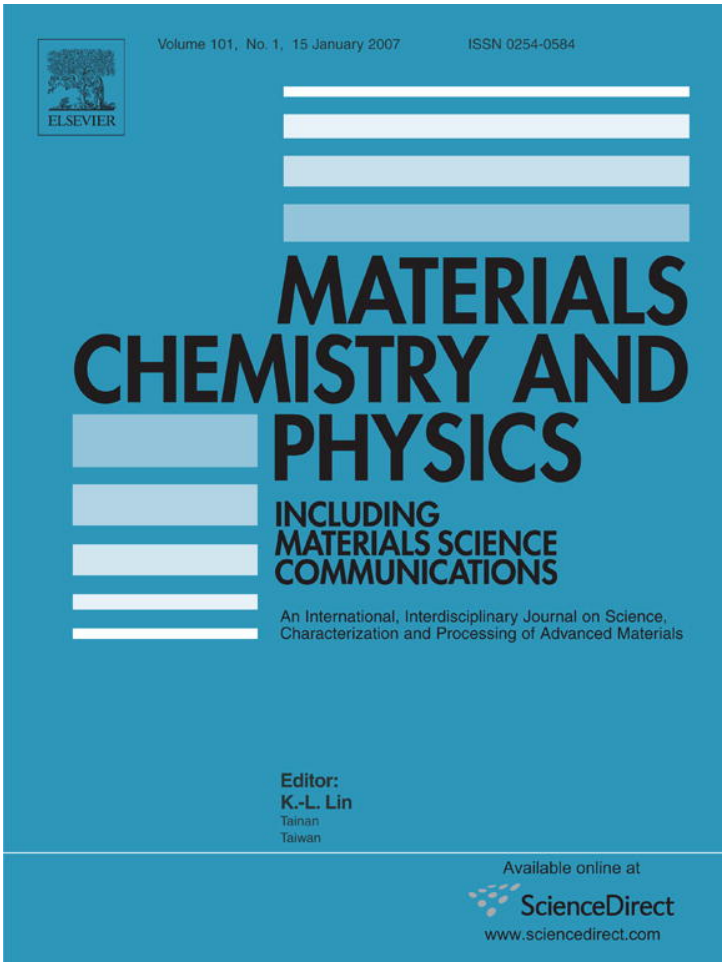

Available online at www.sciencedirect.com
ScienceDirect
Materials Chemistry and Physics 101 (2007) 163–169
MATERIALS CHEMISTRY AND PHYSICS
www.elsevier.com/locate/matchemphys

Role of boric acid in synthesis and tailoring the properties of calcium aluminate phosphor

D. Haranath [a,*], Pooja Sharma [a,*,1], Harish Chander [a], Anwar Ali [b], Nitesh Bhalla [a,2], S.K. Halder [a]

[a] *National Physical Laboratory, Dr. K.S. Krishnan Road, New Delhi 110012, India*
[b] *Department of Chemistry, Jamia Milia Islamia, New Delhi 110025, India*

Received 20 July 2005; received in revised form 16 January 2006; accepted 22 March 2006

Abstract

In the present work related to the development of high-luminous blue-emitting calcium aluminate phosphor, the active role of boric acid (H_3BO_3) as a chemical additive is identified. The appropriate usage of H_3BO_3 in defining the crystal structure, morphology and momentous variation in luminescent properties of calcium aluminate long persisting (LP) phosphor is systematically studied and presented. The results attribute two major roles for H_3BO_3; as a flux for promoting the formation of required crystalline phase, when added in the amounts less than 10 mol% and as one of the precursors for the formation of aluminoborate complex when added above 10 mol%. This amount could be treated as a threshold for aluminoborate complex formation. Luminescent studies revealed that out of all phases identified, $CaAl_2O_4$ is the only phase contributing for maximum photoluminescence (PL) augmentation and long persistence (10–12 h) from Eu^{2+} and Nd^{3+} ions, respectively. The relevant chemistry and reaction mechanism involved during solid-state synthesis of rare-earth doped calcium aluminate LP phosphor system have been discussed with greater emphasis on the luminescent properties affected with the addition of boric acid.

PACS: 32.50.+d; 33.50.Dq; 61.10.Nz

Keywords: Phosphors; Aluminates; Luminescence; Persistence

1. Introduction

Eu^{2+}-doped phosphors usually show intense broad-band emission from deep blue to red region of electromagnetic spectrum. The emission occurs due to electronic transition between $4f^7$ ground state and $4f^65d^1$ excited state [1,2]. Since the 5d orbital is exposed to the surrounding ions the radiative transition is highly influenced by the crystal field components. Consequently, the wavelength of maximum emission strongly depends on the type of the host crystal [1,3]. In this regard many host lattices, namely $BaMgAl_{12}O_{19}$ [4], SrB_4O_7 [5], $SrAl_2B_2O_7$ [6], $CaAl_2O_4$ [1,7], etc., were studied for Eu^{2+}-doping that exhibited blue emission ranging from 400 to 450 nm. Further, these phosphors have decay times ranging from nanoseconds to tens of seconds [8] and form important constituents of light emitting devices, fluorescent lamps, plasma display panels and lamps for medical applications. However, for specific dark-vision applications involving signage, intentional blackouts, emergency rescue guidance systems and luminous watches the phosphor with appreciable brightness and long persistence times (at least 5 h) is a fundamental requisite. In late 1990s Eu^{2+}-doped and, Dy^{3+}/Nd^{3+}-co-doped MAl_2O_4 (M = Sr, Ca, Ba) phosphors with persistence times (>5 h) have been reported [7,9]. Fascinated by the techno-commercial applications, many researchers started exploring the dependence of various physico-chemical parameters such as thermal parameters [10], addition of fluxes, etc. [11–14] on the luminescence and long persistence behavior of these phosphors. Green emitting $SrAl_2O_4$: Eu^{2+}, Dy^{3+} phosphor has gained immense attention because of its higher luminous intensity [15–17] and emission color close to the photopic vision of human eye sensitivity [18]. However, synthesis of blue-emitting phosphor with high quantum efficiency and long persistence times (>10 h) remained a challenging task as many interdependent physical, chemical, and thermal processing parameters are well associated with the tailoring of the phos-

* Corresponding authors. Fax: +91 11 25726938.
E-mail addresses: haranath@nplindia.ernet.in (D. Haranath), shr_pooja@yahoo.co.in (P. Sharma).
[1] Currently working at Regional Research Laboratory, Jorhat-785006, India.
[2] Currently working at Unilever Research India, 64 Main Road, Whitefield, Bangalore-560066, India.

0254-0584/$ – see front matter © 2006 Elsevier B.V. All rights reserved.
doi:10.1016/j.matchemphys.2006.03.003

phor properties. During our work on aluminate system, many chemical additives were tried out that influenced the structural and luminescent properties of the long persistent phosphors. Out of all, the usage of H_3BO_3 fascinated us in establishing the tunability of luminescent properties in calcium aluminate phosphor. For instance, with an optimal amount of H_3BO_3, the phosphor maintained its dark persistence for well over 10 h with emission at 440 nm. This is one of the foremost achievements of our work on blue-emitting long persistent phosphor. In the present paper, we report the influence of H_3BO_3 on various properties and chemistry involved during the solid-state reaction.

2. Experimental details

Rare-earth doped calcium aluminate phosphor samples were prepared by solid-state reaction technique. The starting mixture consists of required oxides (Al_2O_3, Eu_2O_3, Nd_2O_3), carbonate ($CaCO_3$) and H_3BO_3. The purity of rare-earth oxides used is 99.9% and have been obtained from Indian Rare Earths (IRE), while remaining chemicals are AR/GR grade from E-Merck. The molar ratio of the initial composition was fixed at 1:1:0.01:0.02 with respect to $CaCO_3$, Al_2O_3, Eu_2O_3, Nd_2O_3, respectively, to which H_3BO_3 was added from 0 to 40 mol% (with 5 mol% steps) with respect to oxides present in the mixture. The reactants were ball-milled and then sintered at 1100–1300 °C for 2–5 h under mild reducing atmosphere. The final composition of the calcium aluminate phosphor was estimated using Brucker-AXS D8 advance X-ray diffractometer (XRD). The thermogravimetric (TG) and differential thermal analysis (DTA) of starting composition was done using TGA analyzer of METTLER TOLEDO STAR system. The morphological and compositional studies were done using LEO 440 scanning electron microscope (SEM) coupled with energy dispersive detector (EDX-ISIS 300 Oxford). The photoluminescence (PL) spectra were recorded using excitation maxima of 327 nm, with Perkin-Elmer luminescence spectrometer (LS-55). The phosphorescence decay was measured on time base by collecting total light output on a photomultiplier tube (EMI 9658), after turning off the 500 W halogen lamp, which is the source of excitation in the present case. All measurements were performed at room temperature (~25 °C). For persistence measurements, we did set a cut-off limit for luminance level at 0.32 mcd m^{-2}, which is 100 times higher than the minimum perception limit (0.0032 mcd m^{-2}) of light for a dark-adapted human eye [19].

3. Results and discussion

The phosphor with high-luminous intensity and long persistence times (>5 h) is a fundamental requisite for many practical display applications. During our pursuit on development of an efficient blue-emitting long persisting phosphor, it was observed that the luminescence of the fired product varied significantly with respect to the amount of boric acid added. Therefore, in order to appraise and establish the systematic effect related to the addition of H_3BO_3 to the initial oxide mixture, we took three representative samples from a set of more than 15 samples in the present study. The samples with 0, 10 and 30 mol% boric acid additions were named as CAB_0, CAB_{10} and CAB_{30}, respectively, and studied for its structural, morphological and luminescence properties.

3.1. Thermogravimetric analysis

Before proceeding for the customary heat treatment and phase identification of the fired product, it is always necessary to know about the nature of the constituents, their reactivity, decomposition and phase transition temperatures etc. In order to observe these changes thermogravimetric (TGA) and differential thermal (DTA) analyses of the representative samples CAB_0, CAB_{10} and CAB_{30} were carried out (Fig. 1). The initial weight-loss in the region I indicates the removal of adsorbed moisture and further weight-loss in the region I with regard to TGA curves of CAB_{10} and CAB_{30}, represent the gradual dehydroxylation and crystallization processes of H_3BO_3. This is further evidenced by the corresponding endothermic peak located at 110 °C on DTA curve. The difference in peak width distribution of these two curves is due to the variation of H_3BO_3 content present in the initial mixtures. It has also been is identified that with an increase in H_3BO_3 content up to 30 mol%, the reaction threshold of $CaCO_3$ and Al_2O_3 has decreased almost by 60 °C. The endothermic peaks of TGA curves observed in the temperature range 750–810 °C (region II) clearly indicate the decrease in decomposition of $CaCO_3$. The slight weight-loss above 900 °C is attributed to structural relaxation, allowing the mixture to approach the configuration characteristics of the metastable or molten fluid [20]. The structural relaxation occurs primarily by the diffusion motion of the precursor materials. The changes observed on DTA curve in the temperature range 1080–1120 °C (region III) are attributed to viscosity of the molten fluid and crystallization phase formation with minimal weight-loss. Moreover, an endothermic peak was observed only on DTA curve of CAB_{30} in the region >1150 °C. This anomaly may be due to irreversible process in which excess free energy decreases through bond restructuring of excess boron in the crystal structure.

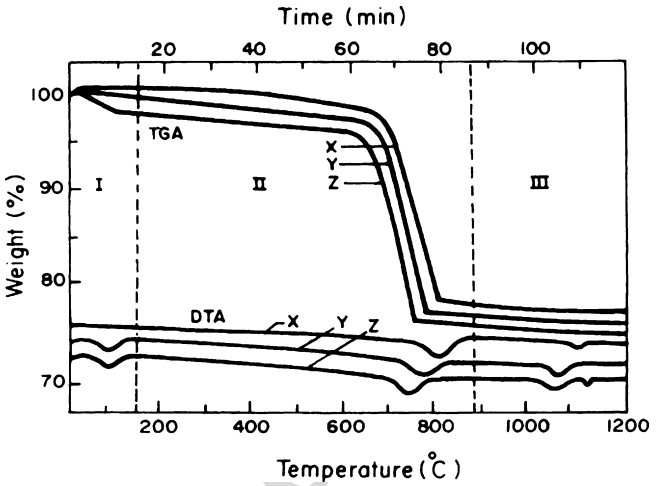

Fig. 1. TGA–DTA curves of calcium aluminate system for the samples (X) CAB_0, (Y) CAB_{10} and (Z) CAB_{30}.

3.2. XRD phase analysis

Fig. 2(a)–(c) represents the XRD profiles of various calcium aluminate phases. The results indicate that all the samples did possess the $CaAl_2O_4$ phase but its presence as major or minor proportion was invariably determined by the amount of H_3BO_3 present in the initial oxide mixture. It is observed that at about 10 mol% H_3BO_3, $CaAl_2O_4$ is the only dominating phase existed as shown in Fig. 2(b). This may be due to the fluxing action of H_3BO_3 that in appropriate amounts (~10 mol%) facilitated the total suppression of other minor phases. Some very remarkable results were obtained when the H_3BO_3 amount

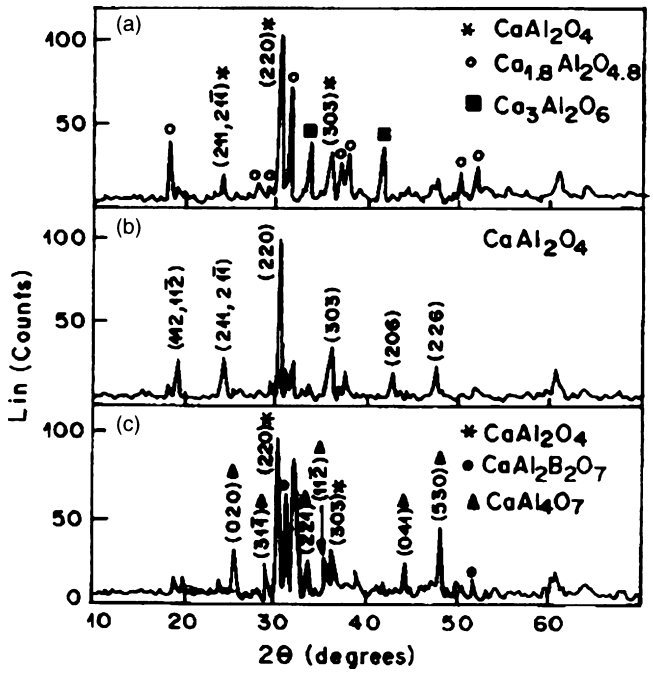

Fig. 2. XRD patterns of calcium aluminate system for the samples (a) CAB_0, (b) CAB_{10} and (c) CAB_{30}.

is increased beyond 10 mol%. The amount of $CaAl_2O_4$ phase began to decrease and the other phases like $CaAl_4O_7$ and $CaAl_2B_2O_7$ started appearing with their corresponding diffraction peaks (Fig. 2(c)). In other words, it can be said that an amount equivalent to 10 mol% H_3BO_3 can be treated as threshold for borate complex phase initialization. Further addition of H_3BO_3 (>40 mol%) resulted in complete dominance of calcium aluminoborate phase over all other calcium aluminate phases. Thus, it is ascertained that H_3BO_3 acts as one of the precursor materials above 10 mol% addition, mitigating the solid solubility of boron in calcium aluminate lattice. These results are consistent with the work published by Pascoal et al. [21] who were successful in preparing monolithic calcium aluminoborate phase for γ-irradiation studies.

3.3. Solid solubility of boron in strontium and calcium aluminate lattices

There are several reports that describe boron as a flux in strontium aluminate phosphor when added <30 mol% [12–14]. But, to the best of our knowledge the effect of boron or its compounds have not been studied in calcium aluminate phosphor. The present study is an attempt to uncover and understand the role of H_3BO_3 in the later system. The dual role of H_3BO_3 (as flux and precursor) was identified on either side of the threshold limit (~10 mol%), as described earlier. The reason for this nature is due to lower thermal stability of $CaCO_3$ (decomposition temperature = 817 °C) than $SrCO_3$ (decomposition temperature = 1258 °C) [22], which allows the formation of molten mixture at low temperature. Therefore, the possibility of solid solubility of boron compounds in calcium aluminate is higher than strontium aluminate systems.

3.4. Solid-state reaction mechanism

It is essential to know the mechanism of solid-state reactions during the formation of various calcium aluminate phases due to the presence of H_3BO_3. In conventional synthesis of $CaAl_2O_4$ crystal from respective oxides (without involving fluxes), high temperature firing for >20 h is required that facilitates the melting and reaction of CaO and Al_2O_3 [23,24]. The chemical reaction that facilitates the formation of $CaAl_2O_4$ phase is given here under:

$$CaCO_3 \xrightarrow{900\,^\circ C} CaO \quad (1)$$

$$CaO + Al_2O_3 \xrightarrow{1700\,^\circ C, 3\,h} CaAl_2O_4 \quad (2)$$

However, addition of H_3BO_3 (as flux), drastically reduces the synthesis temperature from 1700 to ~1300 °C for the same duration of 3 h. Initially it was thought that the boric acid promotes only crystallization by acting as a high temperature solvent. But, after certain limit (>10 mol%) its fluxing action gradually disappeared and it explicitly showed the tendency to take part as a reacting component in the chemical reaction as per the following reactions:

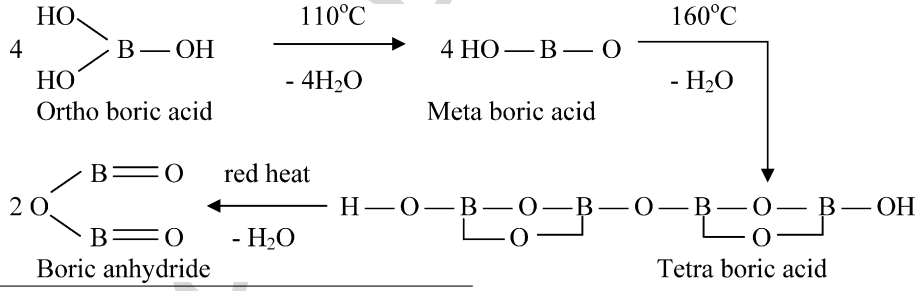

(3)

Upon thermal treatment, B−O−B network of B_2O_3 cleaves to form $B-O^-$ groups via Eq. (4), which in turn, reacts the trigonally coordinated boron to form tetrahedral BO_4 as per the reaction (5):

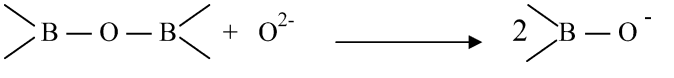

(4)

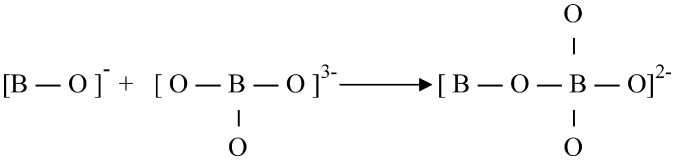

(5)

For excess (~30 mol%) boric acid addition, BO_4^{2-} participates in the formation of superstructure units by breaking of O–Al–O to form O–Al–B bonds. This in turn leads to the formation of $CaAl_2B_2O_7$ phase along with $CaAl_4O_7$ phase. It is important to note that the required MAl_2O_4 (M = Sr/Ca) phase has stuffed tridymite structure [25,26] while $CaAl_2B_2O_7$ has trigonal centrosymmetric structure [6,27].

3.5. SEM observations and EDX analysis

The grain growth and morphological studies along with chemical composition determination was done using SEM coupled with EDX. Fig. 3(a)–(c) represents the SEM micrographs of the samples CAB_0, CAB_{10} and CAB_{30}, respectively. The micrographs clearly indicate the existence of micro/mesopores and grain growth. It is clear from Fig. 3(a) that in the absence of H_3BO_3, irregularly sized and shaped grains with discernible micropores are produced. Also the particle size distribution is reasonably wide ranging from 0.5 to 6 μm. With an addition of H_3BO_3 (up to 10 mol%) particles crystallize to form bigger grains with the prominent appearance of voids, as seen in Fig. 3(b). Further addition of boric acid resulted in smooth grain interfaces with less voids. The grain growth and partial melting morphology for the sample CAB_{30} is seen in Fig. 3(c). A smooth and shiny layer of the particle is indicative of the melting morphology generated by solid-liquid reaction at high temperature. The results are in good agreement with the measured bulk density values, described later.

Fig. 4(a)–(c) illustrates the EDX results of the samples CAB_0, CAB_{10} and CAB_{30}, respectively. Since all the samples exhibit irregular morphology as seen from SEM micrographs the crystalline phase identification becomes difficult. With systematic variation of boric acid, the chemical composition determined by EDX showed a quantitative difference. Although data generated from EDX cannot be used to predict phase composition precisely, it can be correlated with the XRD analysis to draw some conclusions. EDX analysis of the particles in the micrographs of Fig. 3(a)–(c) shows that at.% of Ca with respect to Al is 88, 46 and 22, respectively. These values are found to be close to the Ca/Al ratio of crystal phases attributed for $Ca_{1.8}Al_2O_{4.8}$, $CaAl_2O_4$ and $CaAl_4O_7$ phases, respectively. Thus, the EDX data supports the XRD result of formation of above-mentioned phases in major proportion for the samples CAB_0, CAB_{10} and CAB_{30}, respectively. In other words, EDX analysis further strengthens the role of H_3BO_3 in deciding the lattice structure of the fired product irrespective of its initial composition. The prominent peak of boron at 0.183 keV in Fig. 4(c) for the sample CAB_{30} is the evidence that boric acid is acting as one of the key constituents. This ascertains the fact that the morphology of melting, which is observed in SEM micrograph (Fig. 3(c)) is accompanied by the formation of calcium borate on the surface of calcium aluminate followed by the diffusion of borate ions into aluminates.

3.6. Photoluminescence studies

Fig. 5 represents the photoluminescence (PL) spectra of Eu^{2+} ion in various calcium aluminate host lattices. It is clear from the figure that all the samples gave emission at 440 nm but its intensity varied with the H_3BO_3 content. It is well known that if the crystallization is done properly, it is the flux that facilitates the entry of activator into the crystal lattice and aids in the formation of luminescent center [28]. In the present study the discernible change in the PL intensity can be mainly attributed to the amount of H_3BO_3 and its influence on required crystalline phase ($CaAl_2O_4$) formation and enhanced luminescent properties. From Fig. 5 it is seen that the PL intensity is maximum

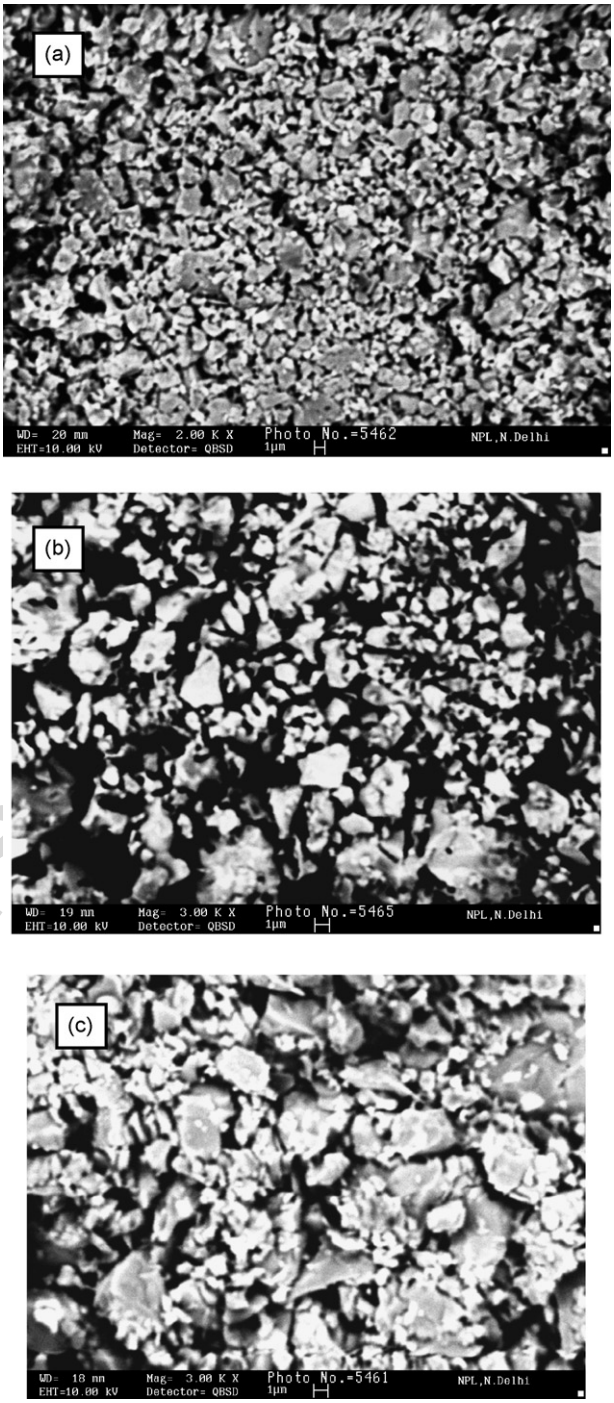

Fig. 3. Comparison of SEM microstructures for the samples (a) CAB_0, (b) CAB_{10} and (c) CAB_{30}.

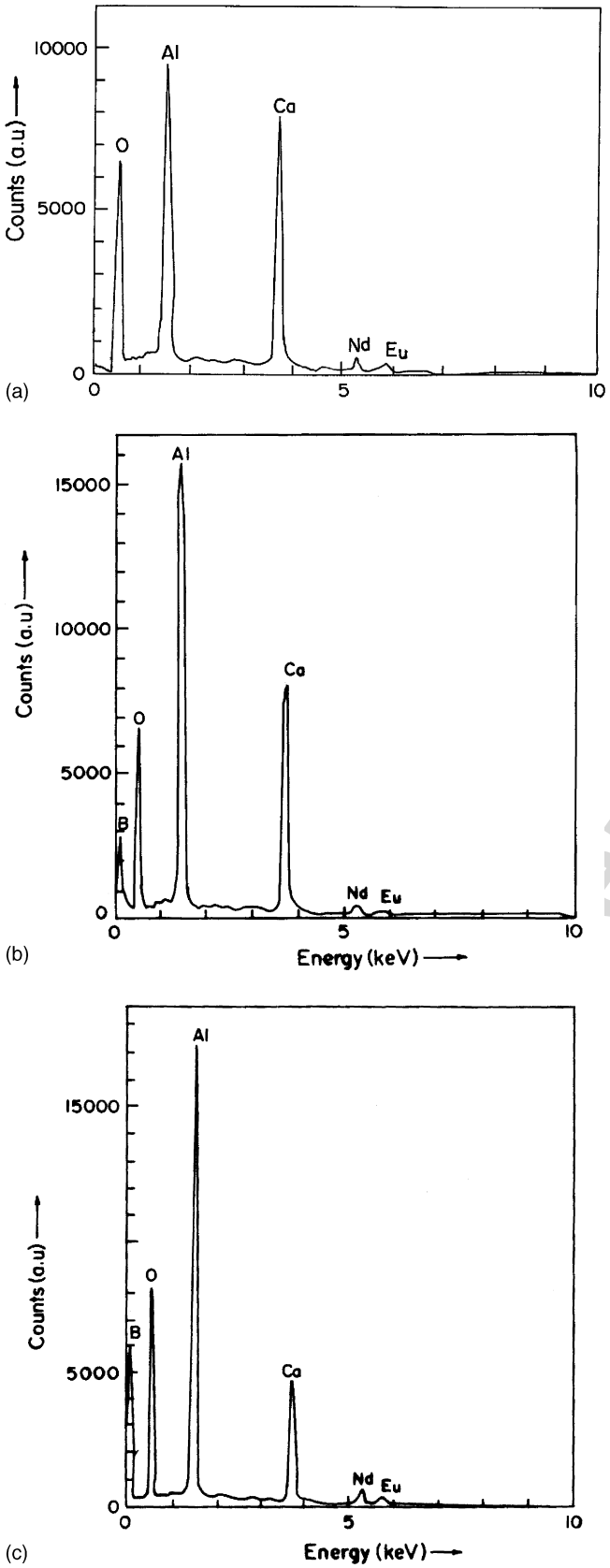

Fig. 4. EDX data of the samples (a) CAB_0, (b) CAB_{10} and (c) CAB_{30}.

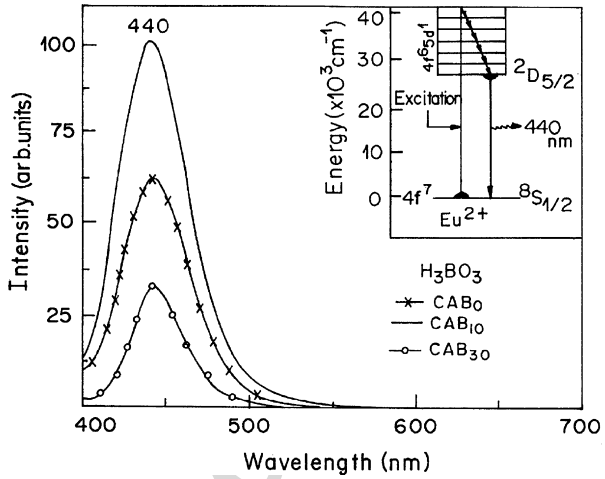

Fig. 5. Photoluminescence spectra of $CaAl_2O_4$: Eu^{2+}, Nd^{3+} phosphor with different H_3BO_3 contents. The inset shows the electronic transitions in Eu^{2+} ion.

for CAB_{10} while in CAB_0 and CAB_{30} samples it is low as $CaAl_2O_4$ phase is present in minor proportion. The reason for maximum PL in $CaAl_2O_4$ system is explained as follows. The $4f \leftrightarrow 5d$ electronic transition of Eu^{2+} ion is associated with the change in electric dipole i.e. $^8S_{7/2} \leftrightarrow {}^2D_{5/2}$, which is a Laporte allowed transition. Because of strong crystal field effect of stuffed tridymite $CaAl_2O_4$ structure, the $4f^65d^1$ level of Eu^{2+} ion completely overlaps the $4f^7$ level, except for the ground state [29]. Therefore, the Eu^{2+} emission takes place from the lowest excited $4f^65d^1$ level lies in the visible region (440 nm) of the electromagnetic spectrum as shown in inset of Fig. 5. Furthermore, it supports our argument that the other phases evolved in the study viz. $Ca_{1.8}Al_2O_{4.8}$, $Ca_3Al_2O_6$ and $CaAl_2B_2O_7$ must be contributing to non-radiative transitions [30]. This may be the reason that the samples CAB_0 and CAB_{30} having major portion of these phases found to show less PL. Fig. 6 depicts the variation in PL intensity of calcium aluminate phosphor with respect to H_3BO_3 content. It is observed that there is a steep increase of photoluminescence intensity with the addition of H_3BO_3 up to ~10 mol%. After that a gradual drop in intensity was observed

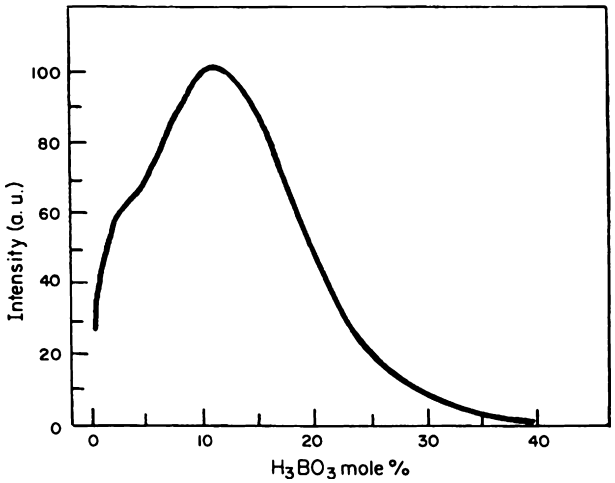

Fig. 6. Variation of PL intensity in calcium aluminate phosphors with H_3BO_3 content ranging from 0 to 40 mol%.

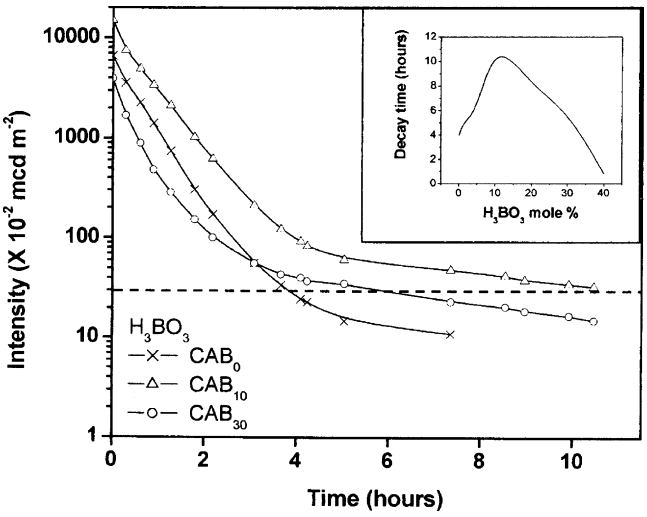

Fig. 7. Decay patterns of various calcium aluminate phosphors. The inset shows the Eu^{2+} decay lifetimes as a function of H_3BO_3. The broken line indicates the cut-off limit set by us at 0.32 mcd m^{-2}.

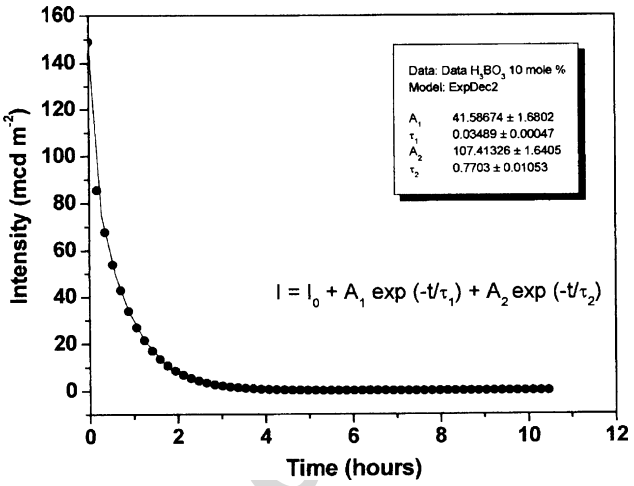

Fig. 8. Simulated decay pattern of CA phosphor with optimized amount (~10 mol%) of H_3BO_3. The inset represents the list of parameters generated from fitting. Dots indicate the actual data points and line the fitting.

due to the formation of non-luminescent Aluminoborate phases described above. Therefore, ~10 mol% H_3BO_3 can be treated as an optimum amount for achieving phosphor with maximum brightness levels.

3.7. Persistence behavior

Fig. 7 shows the persistence (afterglow) pattern of three representative samples having 440 nm Eu^{2+} luminescence on time base. Since, the intensity drops very fast in first few minutes, the PL brightness was recorded on a logarithmic scale. The persistence data was recorded after instantaneous turning off the excitation source. We found that Eu^{2+} persistence time from H_3BO_3-free calcium aluminate phosphor is the lowest with a value of ~4 h with respect to the cut-off limit described in the experimental section. As the amount of H_3BO_3 increased to ~10 mol%, the Eu^{2+} photoluminescence persistence time increased and attained a maximum value of about 11 h. This is the longest perceptible time reported so far for this phosphor. Further increase in boric acid, >30 mol%, resulted phosphors with decreased persistence times of about 5–6 h. However, this value is still higher to the phosphor synthesized without boric acid. The broken line in Fig. 7 represents the cut-off limit (0.32 mcd m^{-2}) set by us, which is also a standard value accepted by escape route marking industries for making sign boards. The dependence of persistence time with respect to H_3BO_3 content is summarized in the inset of Fig. 7.

It is well known that long persistence behavior of rare-earth doped and co-doped MAl_2O_4 system is due to the presence of hole-traps at optimal depth in association with electron centers [7]. Although several models have been reported to explain the long persistence behavior of these phosphors, the exact mechanism has not been elucidated so far [31,32]. The most plausible and accepted mechanism, at present, is based on the presence of lattice defects in rare-earth doped aluminate phosphors [33]. It states that the anion vacancy is already present in aluminate phosphor, which leads to formation of F^+ color center. Whereas, the Nd_2O_3 added in $CaAl_2O_4$ is responsible for cation vacancy formation through charge compensation. This can be explained as $2R^{3+} + 3O^{2-} = 2Ca^{2+} + 3O^{2-} + V_{Ca}$. It is known that enhanced luminescence is due to the introduction of additional cation vacancies. Because of the electrostatic interaction between the highly charged R^{3+} ion and the cation vacancy, which is negative in respect with a regular Ca^{2+} site, the two lattice defects are expected to cluster, and, possibly also with the anion vacancies and the emitting Eu^{2+} ion. The clustering of the R^{3+} ion and the cation vacancy would modify the properties, e.g. the depth of the hole formed by the cation vacancy. However, thermoluminescence is an important tool to ascertain the nature and concentration of the hole-trap levels. To quantitatively ascertain the density, nature and depth of trapping levels thermoluminescence (TL) studies of $CaAl_2O_4$: Eu^{2+}, Nd^{3+} phosphors are in progress.

However, variation in persistence times (Fig. 7) reflects the presence of hole-traps at different depths in different samples [29]. In order to explore the reason for long persistence behavior of CAB_{10} phosphor, the afterglow curve is simulated using exponential decay fit (Fig. 8). The inset of the figure represents the list of parameters generated from the exponential decay fit based on following equation [34]:

$$I = I_0 + A_1 \exp\left(-\frac{t - t_0}{\tau_1}\right) + A_2 \exp\left(-\frac{t - t_0}{\tau_2}\right) \quad (6)$$

where I represents the PL intensity; I_0, A_1, A_2 and t_0 the constants; t the time; and τ_1 and τ_2 are the decay constants. The experimental data fits in the above double-exponential decay equation very well. It is clear from the data that there exist two kinds of trapping levels. The higher PL intensity is attributed to shallow traps of the first kind while longer persistence times (~10–12 h) is attributed to large number of deeper traps of the second kind. But again it is mentioned that better information regarding the nature and concentration of hole-trap levels can be

obtained by the TL studies only and the research work is under progress for the same.

4. Conclusion

In summary, it is to be noted that H_3BO_3 has two major roles in synthesizing an efficient blue phosphorescent material that is best suited for many practical display applications. In the lower (<10 mol%) addition range, H_3BO_3 acts as a fluxing agent in monitoring $CaAl_2O_4$ phase formation whereas, in the higher (>10 mol%) range it behaves as one of the reactants and produces aluminoborate complexes. The formation of various calcium aluminate and aluminoborate phases is discussed. The phosphorescent characteristics are significantly influenced by the addition of small quantities of H_3BO_3 (as low as 1 mol%) in the starting mixture and maximum PL is observed for ∼10 mol%. The persistence of Eu^{2+} afterglow was about 10–12 h, which is relatively higher than the value reported so far.

Acknowledgment

One of the authors' (PS) gratefully acknowledges the Council of Scientific and Industrial Research (CSIR), India, for providing financial assistance to carryout this work under Senior Research Fellowship scheme (No. 31/1/212/2003 EMRI-I).

References

[1] F.C. Palilla, A.K. Levine, M.R. Tomkus, J. Electrochem. Soc. 115 (1968) 642.
[2] M.L. Ruiz-Gonzalez, et al., J. Mater. Chem. 12 (2002) 1128.
[3] V. Abbruscato, J. Electrochem. Soc. 118 (1971) 930.
[4] A.L.N. Stevels, A.D.M. Schrama-de-Pauw, J. Electrochem. Soc. 123 (5) (1976) 691.
[5] K. Machida, G. Adechi, J. Shiokawa, J. Lumin. 21 (1979) 101.
[6] F. Lucas, S. Jaulmes, M. Quarton, T. Le Mercier, F. Guillen, C. Fouassier, J. Solid State Chem. 404 (2000) 150.
[7] T. Matsuzawa, Y. Aoki, N. Takeuchi, Y. Murayama, J. Electrochem. Soc. 43 (80) (1996) 2670.
[8] G. Blasse, B.C. Grabmaier, Luminescent Materials, Springer, Berlin, 1994.
[9] Y. Lin, Z. Tang, Z. Zhang, C. Nan, J. Eur. Ceram. Soc. 23 (2003) 175.
[10] D. Haranath, V. Shanker, H. Chander, P. Sharma, J. Phys. D: Appl. Phys. 36 (2003) 2244.
[11] T. Katsumata, T. Nabae, K. Sasajima, S. Kumuro, T. Morikawa, J. Am. Ceram. Soc. 81 (1998) 413.
[12] I.C. Chen, T.M. Chen, J. Mater. Res. 16 (2001) 644.
[13] D. Wang, Q. Yin, Y. Li, M. Wang, J. Electrochem. Soc. 149 (2002) H65.
[14] J. Nittykoski, T. Aitasalo, J. Hols, H. Junger, M. Lastusaari, M. Parkkinen, M. Tukia, J. Alloys Compd. 374 (2004) 108.
[15] D. Ravichandran, S.T. Johnson, S. Erdei, R. Roy, W.B. White, Displays 19 (1999) 197.
[16] T. Katsumata, T. Nabae, K. Sasajima, T. Matsuzawa, J. Cryst. Growth 183 (1998) 361.
[17] T. Aitasalo, P. Deren, J. Holsa, H. Jungner, J.C. Krupa, M. Latusaari, J. Legendziewiez, J. Nittykoski, W. Strek, J. Solid State Chem. 171 (2003) 114.
[18] S.M. Sze, Physics of Semiconductor Devices, 2nd ed., John Wiley, Singapore, 1999.
[19] Phosphor Research Society (Ed.), Phosphor Handbook, CRC Press, New York, 1998, p. 655.
[20] G.W. Scherer, Relaxation in Glasses and Composites, Wiley, NY, 1986.
[21] H.B. Pascoal, W.M. Pontuschka, H. Rechenberg, J. Non-Cryst. Solids 258 (1999) 92.
[22] P.C.L. Thorne, E.R. Roberts, Inorganic Chemistry, Oliver and Boyd, London, 1954, 829 pp.
[23] D.A. Jerebtsov, G.G. Milchailov, Ceram. Int. 27 (2001) 25.
[24] J.T.C. Van Kemenade, G.P. Hoeks, Abstracts 607, The Electrochemical Society Extended Abstracts, vol. 83-1, San Francisco, CA, May 8–13, 1983, p. 914.
[25] A. Nag, T.R.N. Kutty, Mater. Res. Bull. 39 (2004) 331.
[26] S.H.M. Poort, W.P. Blokpoel, G. Blasse, Chem. Mater. 7 (1995) 1547.
[27] K.S. Chang, D.A. Keszler, Mater. Res. Bull. 33 (1998) 299.
[28] G.F.J. Garlick, Luminescent Materials, Oxford University Press, UK, 1949, 73 pp.
[29] G. Blasse, A. Brill, Philips Tech. Rev. 31 (1970) 303.
[30] D. Haranath, P. Sharma, H. Chander, J. Phys. D: Appl. Phys. 38 (2005) 371.
[31] A. Halperin, in: K.A. Gscneidner Jr., L. Eyring (Eds.), Handbook Phys. Chem. Rare Earths, vol. 28, Elsevier, Amsterdam, 2000 [Chapter 179].
[32] W. Zia, H. Yuan, S. Holmstrom, H. Liu, W.M. Ren, J. Lumin. 83–84 (1999) 465.
[33] J. Holsa, T. Aitasalo, H. Jungner, M. Lastusaari, J. Nittykoski, G. Sapno, J. Alloys Compd. 1–2 (374) (2004) 56.
[34] C. Cheng, D. Mao, J. Shen, C. Feng, J. Alloys Compd. 348 (2003) 224.